

Asteroseismology of the DAV star R808

Y. H. Chen^{1,2,3*} and H. Shu^{1,2}

¹*Institute of Astrophysics, Chuxiong Normal University, Chuxiong 675000, China*

²*School of Physics and Electronical Science, Chuxiong Normal University, Chuxiong 675000, China*

³*Key Laboratory for the Structure and Evolution of Celestial Objects, Chinese Academy of Sciences, P.O. Box 110, Kunming 650011, China*

Accepted:

ABSTRACT

The DAV star R808 was observed by 13 different telescopes for more than 170 hours in April 2008 on the WET run XCOV26. 25 independent pulsation frequencies were identified by this data set. We assumed 19 $m = 0$ modes and performed an asteroseismological study on those 19 modes. We evolve grids of DAV star models by WDEC adopting the element diffusion scheme with pure and screened Coulomb potential effect. The core compositions are from white dwarf models evolved by MESA, which are thermal nuclear burning results. Our best fitting model is from the screened Coulomb potential scenario, which has parameters of $\log(M_{\text{He}}/M_*) = -2.4$, $\log(M_{\text{H}}/M_*) = -5.2$, $T_{\text{eff}} = 11100\text{ K}$, $M_* = 0.710 M_{\odot}$, $\log g = 8.194$, and $\sigma_{\text{RMS}} = 2.86\text{ s}$. The value of σ_{RMS} is the smallest among the four existing asteroseismological work. The average period spacing is 46.299 s for $l = 1$ modes and 25.647 s for $l = 2$ modes. The other 6 observed modes can be fitted by $m \neq 0$ components of some modes for our best fitting model. Fitting the 25 observed modes, we obtain a σ_{RMS} value of 2.59 s. Considering the period spacings, we also assume, that at least in one case, we detect an $l = 2$ trapped mode.

Key words: asteroseismology: individual (R808)-white dwarfs

1 INTRODUCTION

Pulsating white dwarfs are g -mode nonradial pulsators with buoyancy acting as restoring force. There are three main groups of pulsating white dwarfs named as GW Vir stars (PNNV stars and DOV stars), V777 Her stars (DBV stars), and ZZ Ceti stars (DAV stars). The GW Vir stars have stellar atmospheres dominated by HeII, C and O lines. The DBV stars have stellar atmospheres dominated by HeI lines and the DAV stars have stellar atmospheres dominated by HI lines. The instability strip for GW Vir stars, DBV stars, and DAV stars are around 100 000 K, 25 000 K, and 12 000 K respectively. There are around 20 GW Vir stars, 40 DBV stars, and 250 DAV stars observed (Córscico et al. 2019). A large number of DAV stars provide rich research objects for asteroseismology.

Asteroseismology is a powerful tool to detect the inner structure of stars by comparing the observed modes with the calculated ones. For nonradial oscillations, an eigen-mode is indicated by 3 indices, k , l , and m (Handler 2013). The index k means the order of radial standing wave. The indices l and m are the subscripts of spherical harmonic function,

where l is the spherical harmonic degree and m is the azimuthal order. Because of the geometric cancellation effect (Dziembowski 1977), the large l modes have small amplitudes and are not easy to be detected. Therefore, the l values of most observed modes for DAV stars are usually 1 or 2 (Castanheira & Kepler 2008, and references therein). Due to the rotational frequency splitting, $l = 1$ modes show triplets and $l = 2$ modes show quintuplets. Brickhill (1975) derived an approximate relation between the rotation frequency (Ω) and corresponding frequency splitting values ($\delta\nu_{k,l,m}$) for high-overtone ($k \gg 1$) modes and slow rotation as

$$\delta\nu_{k,l,m} = \delta m(1 - C_{k,l})\Omega, \quad (1)$$

where the coefficient $C(k, l) \approx 1/(l(l+1))$ for g -modes. There is a summary on the regularities between the periods and frequencies of g - and p -modes in Bognár et al. (2015). In Eq. (1), m are integers from $-l$ to l , being $-1, 0, 1$ for $l = 1$ modes and $-2, -1, 0, 1, 2$ for $l = 2$ modes.

On the contrary, the observed triplet modes can be identified as $l = 1$ modes and the observed quintuplet modes can be identified as $l = 2$ modes. In addition, the triplet frequency splitting is related to the quintuplet frequency

* E-mail: yanhuichen1987@126.com

splitting by

$$\frac{\delta\nu_{k,1}}{\delta\nu_{k,2}} = 0.6. \quad (2)$$

The relationship is very important for mode identifications. The theory of asteroseismology indicates that the high k g-modes have almost uniform period spacings for successive k modes (same l values). Winget et al. (1981) first proposed that the trapped modes would jump out of the uniform period spacing queue and produce smaller period spacings. These basic laws are helpful for mode identifications. Many pulsating white dwarfs exhibit combination frequencies, which are considered to be derived from the non-linear mixing of sinusoidal signals associated with the mother frequencies. When the stellar convective zone undergoes pulsations, the depth of the convective zone will change with the temperature. Therefore, the combination frequencies have the opportunity to be used for mode identifications (Wu 2001, Kerkwijk et al. 2000).

In order to minimize the gaps in the data sets of rapid variable stars caused by the rotation of the Earth, Nather et al. (1990) organized the Whole Earth Telescope (WET). This instrument provides data of continuity for pulsating white dwarfs. The WET runs, together with some other multi-site observations, have increased the independent observed modes of some DAV stars from a few to a dozen or even more, such as G29-38 (Kleinman et al. 1998), EC14012-1446 (Provencal et al. 2012), HL Tau 76 (Dolez et al. 2006), G38-29 and R808 (Thompson et al. 2009), and so on. The rich observed modes are both opportunities and challenges for model fittings. A large number of reliable identified modes can undoubtedly constrain the fitting model more effectively. However, there are many observed modes that are not easy to be identified. In particular, the modes with small differences in frequencies bring challenges to the mode identification, and increase the uncertainty of model fittings.

The DAV star R808, as one of the WET targets, was observed by 13 different telescopes for more than 170 hours between April 4 and April 17, 2008. Thompson et al. (2009) analyzed the time series photometry on R808 and identified 25 independent pulsation modes. In this paper, we present the preliminary asteroseismological study of R808. In Sect. 2, we perform an analysis of the observed modes of R808. We show the input physics and model calculations in Sect. 3. The model fitting work is displaced in Sect. 4 and the analysis of the fitting results is displaced in Sect. 5. Then, we give a discussion and conclusions in Sect. 6.

2 AN ANALYSIS OF THE OBSERVED MODES OF R808

The DA white dwarf R808 was first identified by McGraw et al. as a DAV star through four nights observations in 1975 at McDonald Observatory (McGraw et al. 1976). R808 was one of the targets of the WET run denoted as XCOV26 in April 2008 (Thompson et al. 2009). The WET runs, together with multi-site observation campaigns, planned to measure the light curve and the corresponding eigen frequencies accurately. The light curve and the shapes of pulses are used to study the relationship between the depth of the convection

Table 1. The observed modes of R808 from Thompson et al. (2009). Fre. is the frequencies in μHz and Per. is the corresponding periods in seconds. The frequency intervals of adjacent modes are marked as δF in μHz . The P_{sel} is the selected periods to constrain the fitting models.

ID	Fre. (μHz)	δF (μHz)	Per. (s)	P_{sel} (s)
f_{25}	2472.45		404.457	404.457
f_{24}	1955.93		511.266	511.266
f_{23}	1589.25		629.228	
		7.42		629.228 or 632.179
f_{22}	1581.83		632.179	
f_{21}	1342.07		745.120	745.120
f_{20}	1255.88		796.253	796.253
f_{19}	1186.65		842.707	842.707
f_{18}	1162.48		860.227	860.227
f_{17}	1142.67		875.146	
		4.34		875.146 or 878.479
f_{16}	1138.33		878.479	
f_{15}	1112.71		898.707	898.707
f_{14}	1100.81		908.422	
		3.76		908.422 or 911.534
f_{13}	1097.05		911.534	
		3.78		
f_{12}	1093.27		914.683	
		1.33		
f_{11}	1091.94		915.803	914.683 or 915.803 or/and 922.504
		7.93		
f_{10}	1084.01		922.504	
f_{09}	1049.98		952.398	
		8.88		952.398 or/and 960.527
f_{08}	1041.10		960.527	
f_{07}	988.736		1011.39	1011.39
f_{06}	961.476		1040.07	
		1.827		1040.07 or 1042.05
f_{05}	959.649		1042.05	
f_{04}	937.444		1066.73	1066.73
f_{03}	916.516		1091.09	1091.09
f_{02}	874.160		1143.96	1143.96
f_{01}	406.652		2459.10	2459.10

zone and the temperature. The eigen frequencies are used to the study of asteroseismology.

The theoretical studies show that the depth of the convective zone varies with the temperature of the star and strongly influences the modes. Therefore, pronounced non-linearities and combination modes are present. The combination modes are helpful to the mode identifications. However, there were only 3 combination modes identified by Thompson et al. (2009) for R808. The convection zone fitting technique needs the asteroseismological mode identifications on l and m values.

Thompson et al. (2009) identified 25 independent frequencies, which are list in Table 1 in this paper. We calculate the frequency intervals of some adjacent modes, which are marked as δF in μHz in Table 1. The δF values of $3.76 \mu\text{Hz}$ and $3.78 \mu\text{Hz}$ are very close. But there is no δF values of $3.77/0.6 = 6.28 \mu\text{Hz}$ or $3.77*0.6 = 2.26 \mu\text{Hz}$. At last, we assume most of the observed modes are $m = 0$, $l = 1$ or 2 modes. The fifth column is the selected periods to constrain the fitting models. For periods close in frequencies, we take

Table 2. The grid size and steps table.

Parameters	grid -size	pre -steps	refined -steps
M_*/M_\odot	0.56to0.72	0.01	0.005
T_{eff} (K)	10800to11800	200	50
$\log(M_{\text{He}}/M_*)$	-2.0to-4.0	0.5	0.1
$\log(M_{\text{H}}/M_*)$	-4.0to-10.0	1.0	0.1

any one to constrain the fitting models, such as f_{23} or f_{22} . However, for two periods which are not very close in frequencies, we take one or two to constrain the fitting models, such as f_{09} or/and f_{08} . The modes in the fifth column of Table 1 are used to constrain the fitting models.

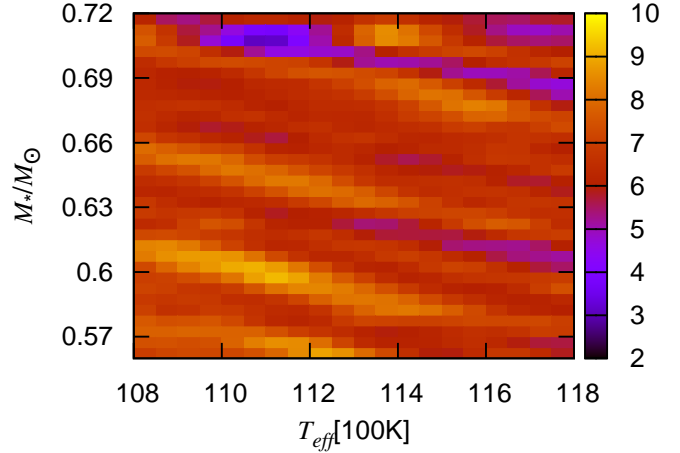
3 INPUT PHYSICS AND MODEL CALCULATIONS

The fifth column of Table 1 contains abundant observed modes. We plan to fit these observed modes using two groups of calculated modes, namely two groups of DAV star models. One group of DAV star models are evolved using the pure Coulomb potential. The other group of DAV star models are evolved using the screened Coulomb potential.

In this work, we evolve a group of main-sequence stars to be hot white dwarfs by MESA code, version number 4298 (Paxton et al. 2011). These white dwarf models have thermal nuclear burning core compositions. We take the core compositions and add them to the seed models of an older version of WDEC. WDEC was first developed by Schwarzschild, which was designed to calculate the evolutions of white dwarfs without previous stellar evolutions (Kutter & Savedoff 1969, Lamb & van Horn 1975, and Wood 1990). WDEC does not calculate the nuclear reaction and mass-loss processes. Therefore, thermal nuclear burning core compositions are helpful to the seed models of WDEC. For WDEC, the equation of state (EOS) are derived by Lamb (1974) and Saumon et al. (1995). The opacities are performed by Itoh et al. (1983, 1984). There is a new version of WDEC (Bischoff-Kim & Montgomery 2018), which directly adopts EOS and opacities of MESA (version number 8118) and contains the stellar oscillation routines. We will apply the new version of WDEC to do asteroseismological research on white dwarfs in the future.

WDEC treats the composition transition zones (C/He and He/H) as the diffusion equilibrium profiles. Su et al. (2014) added the element diffusion scheme of Thoul, Bahcall & Loeb (1994) into WDEC to evolve the time dependent element diffusion DAV star models. The Coulomb logarithm equation is for a pure Coulomb potential with a cutoff at the Debye radius (Thoul, Bahcall & Loeb 1994). Therefore, we mark the method to evolve DAV star models as the pure Coulomb potential scenario.

Thoul, Bahcall & Loeb (1994) used the element diffusion scheme to study the solar interior. Paquette et al. (1986) considered that a screened Coulomb potential would be more suitable for white dwarfs. The Burgers equations of momentum and energy conservation, and the equation of Coulomb logarithm are revised, according to the equations (1, 2, 22-25) of Muchmore (1984). The method adopts the

**Figure 1.** The color residual diagram to fit R808 with DAV star models. Those models are from the screened Coulomb potential scenario with $\log(M_{\text{He}}/M_*) = -2.4$ and $\log(M_{\text{H}}/M_*) = -5.2$. The colors denote the values of σ_{RMS} .

screened Coulomb potential to calculate the element diffusion processes (Cox, Guzik & Kidman 1989). We mark the method to evolve DAV star models as the screened Coulomb potential scenario. For more details, see Chen (2018, 2020).

Two groups of DAV star models are evolved with the methods above. WDEC calculates the C/He and He/H transition zones with pure or screened Coulomb potential. The mixing length parameter is adopted to be 0.6 (Bergeron et al. 1995). Each group of DAV star models are four-parameter grid models, total stellar mass in solar mass M_*/M_\odot , effective temperature T_{eff} , logarithm of helium mass fraction $\log(M_{\text{He}}/M_*)$, and logarithm of hydrogen mass fraction $\log(M_{\text{H}}/M_*)$. The grid size and steps are shown in Table 2. We calculate the theoretical pulsation modes based on the pulsation code of Li (1992a, b).

An equation of root-mean-square residual σ_{RMS} is used to evaluate the fitting results.

$$\sigma_{\text{RMS}} = \sqrt{\frac{1}{n} \sum_n (P_{\text{obs}} - P_{\text{cal}})^2}. \quad (3)$$

In Eq. (3), n denotes the number of fitted observed modes. We reduce the parameter steps around the models with minimum σ_{RMS} values, as shown in the fourth column of Table 2. At last, a best-fitting model will be selected.

4 THE MODEL FITTING WORK OF R808

The 12 modes of f_{25} , f_{24} , f_{21} to f_{18} , f_{15} , f_{07} , f_{04} to f_{01} are assumed to be $m = 0$ modes. First, we fitted the 12 observed modes plus f_{23} , f_{17} , f_{14} , f_{12} , f_{10} , f_{09} , f_{08} , and f_{06} . The observed modes of f_{09} and f_{08} can be fitted by two theoretical modes. We assume both the observed modes of f_{09} and f_{08} to be $m = 0$ modes. However, the observed modes of f_{14} and f_{12} are fitted by the same theoretical mode, which is obviously closer to the observed mode of f_{14} . We

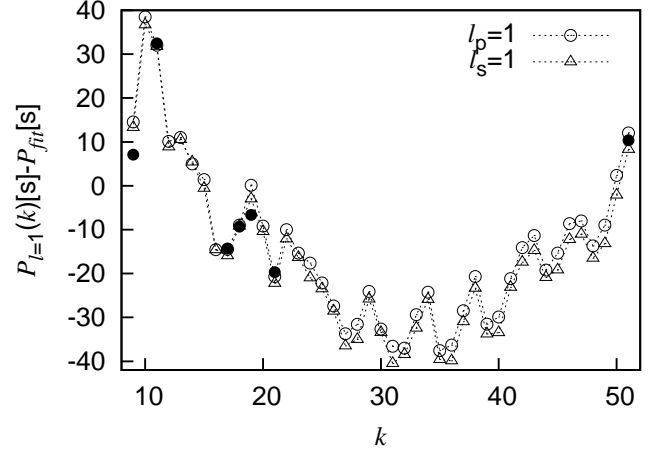
Table 3. The best fitting model parameters for fitting 16 combinations of a total of 19 observed modes.

Combinations of observed modes	$T_{\text{eff}}(\text{K})$	M_*/M_\odot	$\log(M_{\text{H}}/M_*)$	$\log(M_{\text{He}}/M_*)$	$\sigma_{\text{RMS}}(\text{s})$
15 observed modes added	(pure/screened)	(pure/screened)	(pure/screened)	(pure/screened)	(pure/screened)
$f_{23}, f_{17}, f_{14}, f_{06}$	11150/11150	0.705/0.700	-5.2/-5.0	-2.3/-2.4	3.11/2.96
$f_{22}, f_{17}, f_{14}, f_{06}$	11150/11150	0.705/0.700	-5.2/-5.0	-2.3/-2.4	3.24/3.03
$f_{23}, f_{16}, f_{14}, f_{06}$	11150/11100	0.705/0.710	-5.2/-5.2	-2.3/-2.4	3.10/2.96
$f_{22}, f_{16}, f_{14}, f_{06}$	11150/11250	0.705/0.700	-5.2/-5.1	-2.3/-2.3	3.23/3.07
$f_{23}, f_{17}, f_{13}, f_{06}$	11150/11100	0.705/0.710	-5.2/-5.2	-2.3/-2.4	3.09/2.87
$f_{22}, f_{17}, f_{13}, f_{06}$	11150/11100	0.705/0.710	-5.2/-5.2	-2.3/-2.4	3.22/2.98
$f_{23}, f_{16}, f_{13}, f_{06}$	11150/11100	0.705/0.710	-5.2/-5.2	-2.3/-2.4	3.08/2.86
$f_{22}, f_{16}, f_{13}, f_{06}$	11150/11100	0.705/0.710	-5.2/-5.2	-2.3/-2.4	3.21/2.98
$f_{23}, f_{17}, f_{14}, f_{05}$	11150/11150	0.705/0.700	-5.2/-5.0	-2.3/-2.4	3.24/3.06
$f_{22}, f_{17}, f_{14}, f_{05}$	11150/10950	0.705/0.705	-5.2/-5.0	-2.3/-2.5	3.37/3.08
$f_{23}, f_{16}, f_{14}, f_{05}$	11150/11100	0.705/0.705	-5.2/-5.2	-2.3/-2.3	3.23/3.07
$f_{22}, f_{16}, f_{14}, f_{05}$	11150/10850	0.705/0.700	-5.2/-4.8	-2.3/-2.5	3.36/3.09
$f_{23}, f_{17}, f_{13}, f_{05}$	11150/11100	0.705/0.710	-5.2/-5.2	-2.3/-2.4	3.22/2.99
$f_{22}, f_{17}, f_{13}, f_{05}$	11150/11100	0.705/0.710	-5.2/-5.2	-2.3/-2.4	3.35/3.10
$f_{23}, f_{16}, f_{13}, f_{05}$	11150/11100	0.705/0.710	-5.2/-5.2	-2.3/-2.4	3.21/2.99
$f_{22}, f_{16}, f_{13}, f_{05}$	11100/11100	0.710/0.710	-5.2/-5.2	-2.4/-2.4	3.33/3.10

Table 4. The table of detailed fitting results. The model parameters are $\log(M_{\text{He}}/M_*) = -2.4$, $\log(M_{\text{H}}/M_*) = -5.2$, $T_{\text{eff}} = 11100 \text{ K}$, $M_* = 0.710 M_\odot$, and $\log g = 8.194$. P_{obs} is the observed modes, $P_{\text{cal}(p)}/P_{\text{cal}(s)}$ is the calculated modes through the pure/screened Coulomb potential scenario.

P_{obs}	$P_{\text{cal}(p)}$	$P_{\text{obs}}-P_{\text{cal}(p)}$	$P_{\text{cal}(s)}(l, k)$	$P_{\text{obs}}-P_{\text{cal}(s)}$
(s)	(s)	(s)	(s)	(s)
404.457	400.138	4.319	400.261(2,12)	4.196
511.266	518.710	-7.444	517.447(1, 9)	-6.181
629.228	628.784	0.444	628.516(1,11)	0.712
745.120	746.605	-1.485	744.469(2,26)	0.651
796.253	794.457	1.796	793.080(2,28)	3.173
842.707	848.854	-6.147	847.160(2,30)	-4.453
860.227	860.062	0.165	858.589(1,17)	1.638
878.479	877.558	0.921	876.888(2,31)	1.591
898.707	900.077	-1.370	898.874(2,32)	-0.167
911.534	911.891	-0.357	911.677(1,18)	-0.143
922.504	923.219	-0.715	921.378(2,33)	1.126
952.398	952.117	0.281	951.120(2,34)	1.278
960.527	967.259	-6.732	964.172(1,19)	-3.645
1011.39	1011.53	-0.14	1010.66(2,36)	0.73
1040.07	1039.07	1.00	1037.53(1,21)	2.54
1066.73	1063.31	3.42	1061.63(2,38)	5.10
1091.09	1093.54	-2.45	1092.17(2,39)	-1.08
	1096.04	-4.95	1093.96(1,22)	-2.87
1143.96	1142.11	1.85	1140.92(2,41)	3.04
2459.10	2460.75	-1.65	2457.04(1,51)	2.06
σ_{RMS}	3.17 s		2.86 s	

assume both the observed modes of f_{12} and f_{11} to be $m \neq$ components and the observed mode of f_{10} to be $m = 0$ mode. Then, we have the 12 observed modes plus f_{09} , f_{08} , and f_{10} , a total of 15 observed modes with $m = 0$. The 15 observed modes plus f_{23} or f_{22} , f_{17} or f_{16} , f_{14} or f_{13} , f_{06} or f_{05} , a total of 19 observed modes were used to constrain the fitting models. Therefore, n is considered to be 19 in Eq. (3).

**Figure 2.** The diagram to fit $l = 1$ modes. The observed and calculated modes are from Table 4. The filled dots denote the observed modes, which are fitted by $P_{\text{fit}} = 46.2990 \cdot k + 87.4714$. The open dots are calculated from the pure Coulomb potential scenario, while the triangles are calculated from the screened Coulomb potential scenario. The radial order k is adopted to be from 9 to 51.

We use the 15 observed modes plus f_{23} , f_{17} , f_{14} , and f_{06} to preliminarily constrain the fitting models. The pre-best fitting model is from the screened Coulomb potential scenario, and the parameters of the pre-best fitting model are $\log(M_{\text{He}}/M_*) = -2.5$, $\log(M_{\text{H}}/M_*) = -5.0$, $T_{\text{eff}} = 11200 \text{ K}$, $M_* = 0.700 M_\odot$, and $\sigma_{\text{RMS}} = 3.46 \text{ s}$. We reduce the parameter steps around the pre-best model. There are 16 combinations of 15 plus 4 observed modes, as shown in the first column of Table 3. Those best fitting model parameters are very close in Table 3. We chose one with the smallest σ_{RMS} (2.86 s) as the final best fitting model, which is from the screened Coulomb potential scenario. The best fitting model parameters are $\log(M_{\text{He}}/M_*) = -2.4$, $\log(M_{\text{H}}/M_*) = -5.2$, $T_{\text{eff}} = 11100 \text{ K}$, $M_* = 0.710 M_\odot$, and $\log g = 8.194$. With the

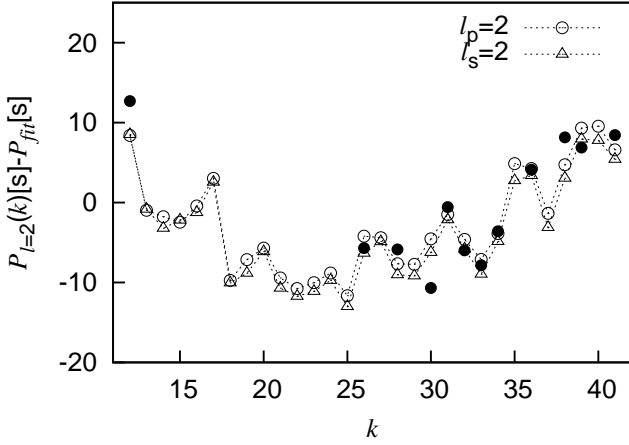


Figure 3. The same as Fig. 2, but for $l = 2$ modes. The fitting function is $P_{fit} = 25.6468 * k + 84.0009$. The radial order k is adopted to be from 12 to 41.

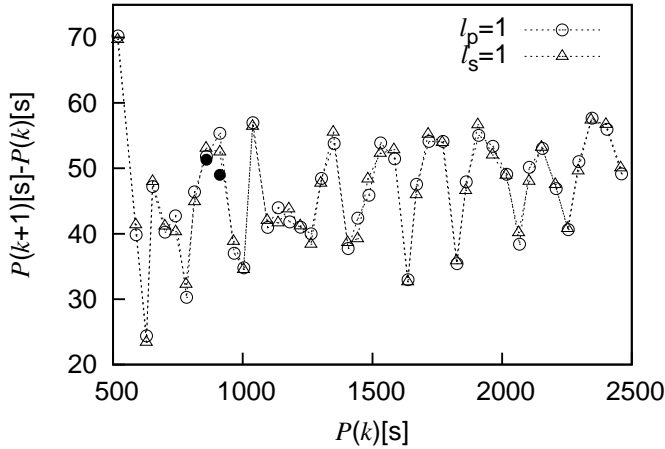


Figure 4. The period to period spacing diagram for $l = 1$ modes. The radial order k is adopted to be from 9 to 51.

fixed helium and hydrogen mass fraction of $\log(M_{\text{He}}/M_*) = -2.4$ and $\log(M_{\text{H}}/M_*) = -5.2$, we show the color residual diagram to fit R808 in Fig. 1. It is obvious that the best fitting model has $T_{\text{eff}} = 11100$ K and $M_* = 0.710 M_{\odot}$.

We show the detailed fitting results in Table 4. The observed modes of f_{23} , f_{16} , f_{13} , and f_{06} are assumed to be $m = 0$ modes, according to the best fitting model. There are 19 observed modes in the first column of Table 4. The second column are the calculated modes through the pure Coulomb potential scenario. The fourth column are the calculated modes through the screened Coulomb potential scenario. We show the spherical harmonic degrees and the radial orders in the brackets. There are 7 $l = 1$ modes and 12 $l = 2$ modes. In addition, the f_{03} mode of 1091.09 s can be fitted by 1092.17 s ($l=2$, $k=39$) or 1093.96 s ($l=1$, $k=22$). The corresponding P_{obs} minus P_{cal} values are calculated for each observed mode.

Fitting the 19 observed modes, σ_{RMS} is 3.17 s/2.86 s for the theoretical modes calculated through the pure/screened

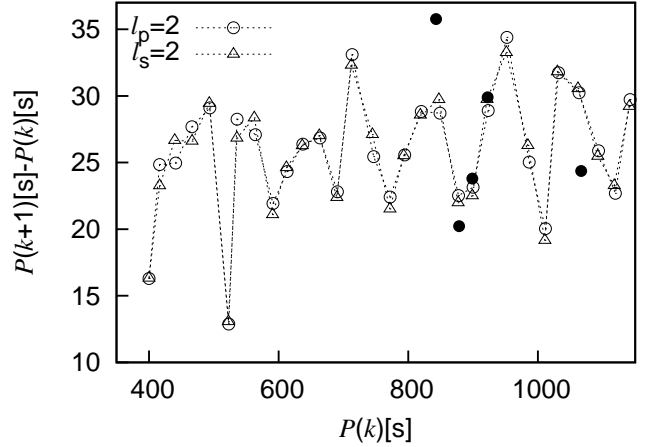


Figure 5. The same as Fig. 4, but for $l = 2$ modes. The radial order k is adopted to be from 12 to 41.

Coulomb potential scenario. From the pure Coulomb potential scenario to the screened Coulomb potential scenario, some observed modes are fitted better obviously such as f_{24} (511.266 s), f_{19} (842.707 s), f_{08} (960.527 s) in Table 4, σ_{RMS} is improved by 9.78%.

In Fig. 2, we show the detailed fitting results for $l = 1$ modes. The radial order k is adopted to be from 9 to 51 in Fig. 2. The average period spacing for $l = 1$ modes is 46.299 s. The filled dots are the observed modes, the open dots are the calculated modes from the pure Coulomb potential scenario, the triangles are the calculated modes from the screened Coulomb potential scenario. Figure 3 is the detailed fitting results for $l = 2$ modes. The radial order k is adopted to be from 12 to 41. The average period spacing for $l = 2$ modes is 25.647 s. The ratio between 46.299 s and 25.647 s is 1.805, which is close to the theoretical value of $\sqrt{3} = 1.732$. In Fig. 4 and 5, we show the period to period spacing diagram for $l = 1$ and 2 modes respectively. For $l = 1$ modes, k is adopted to be from 9 to 51. For $l = 2$ modes, k is adopted to be from 12 to 41. In Fig. 4, we can see that the period spacings are around ~ 45 s. In Fig. 5, we can see that the period spacings are around ~ 25 s.

5 THE PRELIMINARY ANALYSIS OF THE FITTING RESULTS

Fitting the 19 observed modes of R808, σ_{RMS} is improved by 9.78% from the pure Coulomb potential scenario to the screened Coulomb potential scenario. Fitting the 6 observed modes of HS 0507+0434B, σ_{RMS} was improved by 34% from the pure Coulomb potential scenario to the screened Coulomb potential scenario (Chen 2020). In Table 4, Fig. 2, and Fig. 3, we can see that most of the observed modes are basically reduced by around 1 second considering the screened Coulomb potential. If there are a large number of calculated modes which have slightly longer periods than the observed modes, the screened Coulomb potential must be helpful.

In Table 5, we show the best fitting models of the spectral results of Bergeron et al. (2004) and the asteroseismo-

Table 5. Table of best fitting models. The ID number 1 is from the spectral results of Bergeron et al. (2004). The ID number 2, 3, 4, and 5 is from the asteroseismological results of Castanheira & Kepler (2009), Bischoff-Kim (2009), Romero et al. (2012), and the present paper respectively.

ID	T_{eff} (K)	$\log g$	M_* (M_{\odot})	$\log(M_{\text{H}}/M_*)$	$\log(M_{\text{He}}/M_*)$	σ_{RMS} (s)
1	11160 \pm 200	8.04 \pm 0.05	0.626 \pm 0.028			
2	11000		0.65	-9.5	-3.5	5.48
3	11250		0.675	-4.62	-2.58	3.61
4	11213 \pm 130	8.18 \pm 0.05	0.705 \pm 0.033	-4.28 to -4.72	-2.12	4.00
5(s)	11100	8.194	0.710	-5.2	-2.4	2.86

Table 6. The detailed fitting results and a possible mode identification for 25 observed modes based on the best fitting model. The value of σ_{RMS} is 2.59s when fitting the 25 observed modes.

$P_{\text{cal}(s)}(l, k, m)$ (s)	P_{obs} (s)	$P_{\text{obs}} - P_{\text{cal}(s)}$ (s)	$P_{\text{cal}(s)}(l, k, m)$ (s)	P_{obs} (s)	$P_{\text{obs}} - P_{\text{cal}(s)}$ (s)	$P_{\text{cal}(s)}(l, k, m)$ (s)	P_{obs} (s)	$P_{\text{obs}} - P_{\text{cal}(s)}$ (s)
138.729(1,1,0)			160.761(2,3,0)			818.592(2,29,0)		
207.873(1,2,0)			194.745(2,4,0)			847.160(2,30,0)	842.707	-4.453
278.302(1,3,0)			207.271(2,5,0)			867.333(2,31,+2)		
302.893(1,4,0)			227.620(2,6,0)			872.083(2,31,+1)	875.146	3.063
340.082(1,5,0)			267.739(2,7,0)			876.888(2,31,0)	878.479	1.591
393.802(1,6,0)			289.890(2,8,0)			881.741(2,31,-1)		
459.064(1,7,0)			301.182(2,9,0)			886.651(2,31,-2)		
479.819(1,8,0)			339.863(2,10,0)			888.841(2,32,+2)		
517.447(1,9,0)	511.266	-6.181	365.676(2,11,0)			893.831(2,32,+1)		
587.142(1,10,0)			400.261(2,12,0)	404.457	4.196	898.874(2,32,0)	898.707	-0.167
628.516(1,11,0)	629.228	0.712	416.584(2,13,0)			903.979(2,32,-1)		
651.918(1,12,0)			439.837(2,14,0)			909.140(2,32,-2)		
699.910(1,13,0)			466.495(2,15,0)			910.838(2,33,+2)		
741.080(1,14,0)			493.100(2,16,0)			916.078(2,33,+1)	915.803	-0.275
781.394(1,15,0)			522.546(2,17,0)			921.377(2,33,0)	922.504	1.126
813.677(1,16,0)			535.604(2,18,0)			926.741(2,33,-1)		
858.589(1,17,0)	860.227	1.638	562.435(2,19,0)			932.166(2,33,-2)		
908.554(1,18,+1)	908.422	-0.132	590.787(2,20,0)			951.120(2,34,0)	952.398	1.278
911.677(1,18,0)	911.534	-0.143	611.878(2,21,0)			984.379(2,35,0)		
914.821(1,18,-1)	914.683	-0.138	631.453(2,22,+2)	632.179	0.726	1010.66(2,36,0)	1011.39	0.73
964.172(1,19,0)	960.527	-3.645	633.967(2,22,+1)			1016.66(2,37,+2)		
1003.01(1,20,0)			636.500(2,22,0)			1023.20(2,37,+1)		
1037.53(1,21,0)	1040.07	2.54	639.055(2,22,-1)			1029.81(2,37,0)		
1093.96(1,22,0)			641.630(2,22,-2)			1036.52(2,37,-1)		
1136.01(1,23,0)			662.759(2,23,0)			1043.31(2,37,-2)	1042.05	-1.26
1177.67(1,24,0)			689.779(2,24,0)			1061.63(2,38,0)	1066.73	5.10
2457.04(1,51,0)	2459.10	2.06	712.158(2,25,0)			1092.17(2,39,0)	1091.09	-1.08
			744.469(2,26,0)	745.120	0.651	1117.65(2,40,0)		
121.199(2,2,0)			771.570(2,27,0)			1140.92(2,41,0)	1143.96	3.04
121.199(2,2,0)			793.080(2,28,0)	796.253	3.173	1170.13(2,42,0)		

logical results of Castanheira & Kepler (2009), Bischoff-Kim (2009), Romero et al. (2012), and the present paper respectively. Castanheira & Kepler (2009) evolved grids of DAV star models by WDEC with a fixed homogeneous C/O 50:50 core. Bischoff-Kim (2009) calculated the asteroseismological models by WDEC with a parameterized central O abundance and O profiles. Romero et al. (2012) calculated the asteroseismological models by LPCODE with time dependent element diffusion effect. The effective temperature values in Table 5 are basically consistent. The total stellar mass and the gravitational acceleration obtained by this work are basically consistent with those obtained by Romero et al. (2012). The

$\log(M_{\text{H}}/M_*)$ value obtained by this work is slightly smaller than that obtained by Bischoff-Kim (2009) and Romero et al. (2012). The $\log(M_{\text{He}}/M_*)$ value obtained by this work is in the middle between that obtained by Bischoff-Kim (2009) and Romero et al. (2012). Castanheira & Kepler (2009) fitted 8 observed modes of R808 and obtained a σ_{RMS} value of 5.48s. Bischoff-Kim (2009) fitted 18 modes of R808 and obtained a σ_{RMS} value of 3.61s. Romero et al. (2012) fitted 17 modes of R808 and obtained a σ_{RMS} value of 4.00s. We fit 19 modes of R808 and obtain a σ_{RMS} value of 2.86s. The mode identifications (values of k , l , and m) of the observed modes are not exactly same among the four asteroseismo-

logical work. Even in this work, the mode of f_{03} (1091.09) can be fitted by 1092.17 ($l=2, k=39$) or 1093.96 ($l=1, k=22$). More efforts are needed for the detailed mode identifications.

We show the detailed fitting results for the best fitting model in Table 6. The modes of f_{18} (860.227 s), f_{13} (911.534 s), f_{08} (960.527 s) are fitted by modes of $l = 1, k = 17, 18$, and 19 respectively. The corresponding period spacing is 51.307 s and 48.993 s respectively, as shown in Fig. 4, which are larger than the average period spacing for $l = 1$ modes (46.299 s). The modes of f_{19} (842.707 s), f_{16} (878.479 s), f_{15} (898.707 s), f_{10} (922.504 s), f_{09} (952.398 s), f_{04} (1066.73 s), f_{03} (1091.09 s) are fitted by modes of $l = 2, k = 30, 31, 32, 33, 34, 38$, and 39 respectively. The corresponding period spacing is 35.772 s, 20.228 s, 23.797 s, 29.894 s, and 24.36 s respectively, as shown in Fig. 5. The average period spacing for the observed $l = 2$ modes is 25.647 s. Therefore, the modes of f_{16} (878.479 s) and/or f_{15} (898.707 s) may be the trapped modes. However, the thinner the H atmosphere mass, the more obvious the mode trapping effect (Brassard et al. 1992). The H atmosphere mass is not very thin for the last three best fitting models in Table 5 to fit R808.

In Table 4, the mode of f_{13} (911.534 s) is fitted by an $l = 1$ mode. Therefore, we assume that f_{14} , f_{13} , and f_{12} in Table 1 make up a triplet. The value of $\delta\nu_{k,1}$ is $3.77 \mu\text{Hz}$ and The value of $\delta\nu_{k,2}$ is $6.28 \mu\text{Hz}$, according to Eq. (2). In Table 6, the $m \neq 0$ components of some modes are calculated according to the values of $\delta\nu_{k,1}$ and $\delta\nu_{k,2}$, and used to fit the other 6 observed modes in Table 1. The 25 observed modes in Table 1 are fitted in Table 6 with $\sigma_{RMS} = 2.59$ s. The value of $\delta\nu_{k,1} = 3.77 \mu\text{Hz}$ corresponds to a rotational period of 1.54 days for R808. Bischoff-Kim (2009) identified 1 $l = 1$ multiplet and 5 $l = 2$ multiplets. In Table 2 of Bischoff-Kim (2009), they derived $\delta\nu_{k,1} = 3.59 \mu\text{Hz}$ and $\delta\nu_{k,2} = 7.55 \mu\text{Hz}$, $8.87(26.60/3) \mu\text{Hz}$, $9.62 \mu\text{Hz}$, $8.28 \mu\text{Hz}$, and $9.84 \mu\text{Hz}$. Those values of $\delta\nu_{k,2}$ are larger than $\delta\nu_{k,1}/0.6 = 5.98 \mu\text{Hz}$.

6 DISCUSSION AND CONCLUSIONS

The DAV star R808 was observed for 170.28 hours in April 2008 on the WET run XCOV26 (Thompson et al. 2009). There were 25 independent pulsation modes identified. We assume 19 $m = 0$ modes and use them to constrain the fitting models. We add the core compositions of white dwarf models evolved by MESA to WDEC to obtain the thermal nuclear burning core. For the composition transition zones (C/He and He/H), we do not adopt the diffusion equilibrium profiles but element diffusion results. One group of DAV star models are evolved with the element diffusion scheme of pure Coulomb potential (Thoul, Bahcall & Loeb 1994). The other group of DAV star models are evolved with the element diffusion scheme of screened Coulomb potential (Chen 2018, 2020). The pulsating periods of the two groups of DAV star models are calculated and used to fit the 19 observed modes.

A best fitting model is obtained with $\log(M_{\text{He}}/M_*) = -2.4$, $\log(M_{\text{H}}/M_*) = -5.2$, $T_{\text{eff}} = 11100$ K, $M_* = 0.710 M_{\odot}$, and $\log g = 8.194$. From the pure Coulomb potential scenario to the screened Coulomb potential scenario, the root-mean-square residual σ_{RMS} is from 3.17 s to 2.86 s, 9.78% improved. The effective temperature of our best fitting model is basically consistent with that of previous work on R808, as shown in Table 5. In Table 5, we can see that the other

parameters of our best fitting model are basically consistent with that of asteroseismological work of Romero et al. (2012). The value of σ_{RMS} for the present work is smaller than that of asteroseismological work of Castanheira & Kepler (2009), Bischoff-Kim (2009) and Romero et al. (2012).

The observed modes of f_{14} , f_{13} , and f_{12} are possible to be a triplet with $\delta\nu_{k,1} = 3.77 \mu\text{Hz}$. Therefore, the value of $\delta\nu_{k,2}$ is assumed to be $6.28 \mu\text{Hz}$, according to Eq. (2). The $m \neq 0$ components of some modes for our best fitting model are calculated according to the values of $\delta\nu_{k,1}$ and $\delta\nu_{k,2}$, and used to fit the other 6 observed modes in Table 1. Fitting the 25 observed modes, the value of σ_{RMS} is 2.59 s for our best fitting model. The average period spacing is 46.299 s for $l = 1$ modes and 25.647 s for $l = 2$ modes. The modes of f_{16} and/or f_{15} have the minimum period spacings and may be the trapped modes.

7 ACKNOWLEDGEMENTS

The work is supported by the foundations of NSFC of China (Grant No. 11803004 for the asteroseismological study of the screened Coulomb potential on white dwarfs and Grant No. 11563001 for the study of white dwarf pulsations). We are very grateful to X. H. Chen, Q. S. Zhang, and J. Su for their constructive suggestions.

DATA AVAILABILITY

The data underlying this article are available in the article and in its online supplementary material.

REFERENCES

- Bergeron P., Wesemael F., Lamontagne R. et al., 1995, ApJ, 449, 258
- Bergeron P., Fontaine G., Bileres M. et al., 2004, ApJ, 600, 404
- Bischoff-Kim A., 2009, AIPC, 1170, 621
- Bischoff-Kim A., Montgomery M. H., 2018, AJ, 155, 187
- Bognár Zs., Lampens P., Frámat Y., et al., 2015, A&A, 581, A77
- Brassard P., Fontaine G., Wesemael F., et al., 1992, ApJS, 80, 369
- Brickhill A. F., 1975, MNRAS, 170, 405
- Castanheira B. G., Kepler S. O., 2008, MNRAS, 385, 430
- Castanheira B. G., Kepler S. O., 2009, MNRAS, 396, 1709
- Chen Y. H., 2018, MNRAS, 475, 20
- Chen Y. H., 2020, MNRAS, 495, 2428
- Córsico A. H., Althaus L. G., Miller Bertolami M. M., et al., 2019, A&ARv, 27, 7
- Cox A. N., Guzik J. A., Kidman P. B., 1989, ApJ, 342, 1187
- Dolez N., Vauclair G., Kleinman S. J., et al., 2006, A&A, 446, 237
- Dziembowski W., 1977, AcA, 27, 203
- Handler G., 2013, Asteroseismology, Planets, Stars and Stellar Systems Vol. 4, ISBN 978-94-007-5614-4., 207
- Itoh N., Mitake S., Iyetomi H., Ichimaru S., 1983, ApJ, 273, 774

- Itoh N., Kohyama Y., Matsumoto N., Seki M., 1984, *ApJ*, 285, 758
- van Kerkwijk, M. H., Clemens, J. C., Wu Y., 2000, *MNRAS*, 314, 209
- Kleinman S. J., Nather R. E., Winget D. E., et al., 1998, *ApJ*, 495, 424
- Kutter G. S., Savedoff M. P., 1969, *ApJ*, 156, 1021
- Lamb D. Q., 1974, PhD Thesis, The University of Rochester
- Lamb D. Q., van Horn H. M., 1975, *ApJ*, 200, 306
- Li Y., 1992a, *A&A*, 257, 133
- Li Y., 1992b, *A&A*, 257, 145
- McGraw John T., Robinson Edward L., 1976, *ApJ*, 205, L155
- Muchmore D., 1984, *ApJ*, 278, 769
- Nather R. E., Winget D. E., Clemens J. C., et al., 1990, *ApJ*, 361, 309
- Paquette C., Pelletier C., Fontaine G., et al., 1986, *ApJS*, 61, 177
- Paxton B., Bildsten L., Dotter A., Herwig F., Lesaffre P., Timmes F., 2011, *ApJS*, 192, 3
- Provencal J. L., Montgomery M. H., Kanaan A., et al., 2012, *ApJ*, 751, 91
- Romero A. D. Córscico A. H., Althaus L. G., et al., 2012, *MNRAS*, 420, 1462
- Saumon D., Chabrier G., Van Horn H. M., 1995, *ApJS*, 99, 713
- Su J., Li Y., Fu J. -N., Li C., 2014, *MNRAS*, 437, 2566
- Thoul A. A., Bahcall J. N., Loeb A., 1994, *ApJ*, 421, 828
- Thompson S. E., Provencal J. L., Kanaan A., et al., 2009, *JPhCS*, 172, 012067 DOI
- Winget, D. E., Van Horn, H. M., Hansen, C. J. 1981, *ApJ*, 245, 33
- Wood M. A., 1990, PhD Thesis, The University of Texas at Austin
- Wu, Y., 2001, *MNRAS*, 323, 248